JJMIE

Volume 5, Number 5, Oct. 2011
ISSN 1995-6665
Pages 407 - 417

Jordan Journal of Mechanical and Industrial Engineering

Variable Structure Controller Schemes Based on Work and Energy Principle for SIMO Systems

M. Ababneh*,[a], A. Al-Jarrah[a], K. Al-Widyan[a], S. BaniHani[a]

[a]*Mechatronics Engineering Department, Hashemite University,P.O.Box 150459, Zarqa, 13115, Jordan*

Abstract

This paper presents a reasoned methodology for designing variable structure controllers (VSC), also known as sliding mode controllers (SMC), for Single- Input-Multi-output (SIMO) systems. The approach is explicitly based on the assessment of a system total energy, and the realization of a VSC that minimizes that energy. A relationship between controller gains and the slope of the sliding surface is explicitly formulated. The practical implementation of the proposed approach is exemplified on an inverted pendulum system where the system has two independent sliding surfaces representing the two system states. A VSC with hyper sliding surface is also introduced. Since the pendulum system has no dissipative viscous load to absorb energy, a VSC for pure inertial systems is proposed.

Keywords: Work and Energy; Variable Structure Controller; Hyper; SIMO; Inertial system; Optimal

1. Introduction

VSCs or SMCs are based on the theory of Variable Structure Systems (VSS) which first appeared in the late fifties in Russia as a special class of nonlinear systems [1-2]. A VSC is characterized by a discontinuous action whereby upon reaching a switching, or sliding, surface in the state space the structure of the controller changes to another which is a member of a set of possible continuous functions of the state [2]. This approach can result in a very robust control action that is superior to any of the members of the set of controller it is allowed to switch among taken alone.

The realization of a VSC involves two distinct stages; 1) the equation of the sliding surface or the manifold is designed to meet the desired dynamics of the sliding motion in accordance with some performance specifications, 2) the switching or discontinuous feedback control law is designed such that the locus of the system state would reach the manifold and that the sliding mode exists on this manifold. The design of linear sliding mode surfaces for linear systems was studied and developed extensively [3-9]. The design of the sliding surface for more general nonlinear systems remains largely an open problem [1]. This paper focuses exclusively on linear sliding mode surfaces.

Design theory and procedures outlined in [3-9] and other literature dealing with VSCs and SMCs tend to be specific to a narrow class of plant structures. To overcome this drawback, methods developed in other publications [10- 13] involve integrating the classical theories used for designing the sliding mode surface and the switching control law with other computational intelligence-based systems such as Fuzzy Logic (FL), Neural Networks (NN), and Genetic Algorithms (GA). However, despite its simplicity of realization and advantages, the lack of a general systematic design approach that is mathematically lucid have hindered its widespread use. Since all the reported VSC design approaches are specific to the specific system under consideration and tend to exploit its characteristics, rather than being general, the need for such a methodology provided the motivation for this work. Furthermore, literature on the subject does not provide an understanding of the link between the control law parameters suitable for VSCs and the sliding surface parameters.

This paper provides a mathematically clear link between the action of a VSC and the work and energy of the system. This link is used to tie the control law parameters to those of the sliding surface. The stability of a designed system using the proposed methodology is provided. The design methodology is suitable for Single-Input-Single-Output (SISO) as well as Single-Input-Multiple-Output (SIMO) control systems. An inverted pendulum system is selected to test the new design methodology is a SIMO system. The system is a special case of Multi-Input-Multi-output (MIMO) control systems and is acknowledged to be difficult one to control. In order to study the performance of the controller, different VSC schemes are proposed and applied to the pendulum system. Simulation results and comparisons between the designed controllers and classical ones are provided to show the performance of the proposed VSC schemes.

2. VSCs and the Principle of Work and Energy

A phase plane portrait of a system relates a system state to its derivative. For a physical system, the axes of the phase plane are typically the displacement and the

* Corresponding author. e-mail: ababneh@hu.edu.jo

velocity. Consider a conservative spring-mass system subjected to a step input displacement. Upon release, the potential energy is gradually converted to kinetic energy as the body accelerates. The continual interchange between potential and kinetic energy cause the body to oscillate. The ordinate of the system phase portrait being velocity can be viewed as a proxy of the kinetic energy and the abscissa being displacement can be viewed as a proxy of the potential energy. With reference to Figure 1, the total energy, E, of the system is given by:

$$E = \tfrac{1}{2}kx^2 + \tfrac{1}{2}m\dot{x}^2 \quad (1)$$

where m is the system mass and k is the spring constant. Rearranging Equation 1 and using $a = \sqrt{2E/k}$ and $b = \sqrt{2E/m}$ gives:

$$\frac{x^2}{a^2} + \frac{\dot{x}^2}{b^2} = 1 \quad (2)$$

Equation 2 is that of an ellipse. Figure 1 (b) shows a scaled phase portrait of the system where the abscissa is scaled by $1/a^2$ and the ordinate by $1/b^2$. The ellipses correspond to different initial levels E_i. The phase portrait in the figure shows that the system has no dissipative element since its energy level remains constant. A phase plane portrait that converge to the origin indicates a stable system with decreasing energy level and a phase portrait diverging to infinity indicates an unstable system with increasing energy level as shown in Figure 2 (a) and (b) respectively.

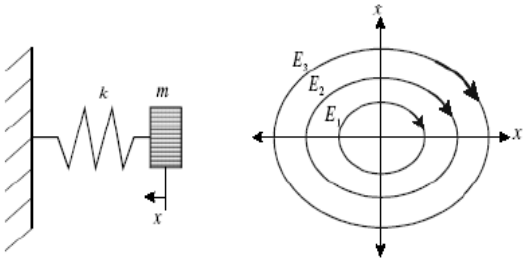

Figure 1: Spring-mass system phase portrait. a) System b) Phase portrait.

A dynamic system converges towards stability if its total energy decreases asymptotically with time to its minimum value at the equilibrium state. Lyapunov criteria exploits this fact by requiring the time derivative of the Lyapunov energy function, be it a true representation of the energy of the system or a proxy for it, to be negative definite.

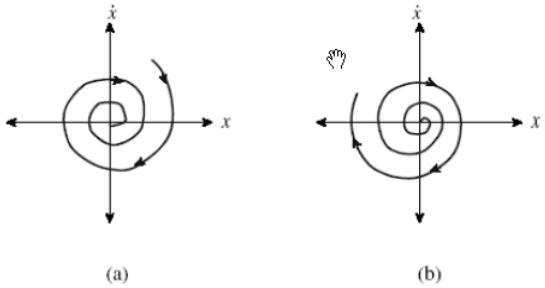

Figure 2: Phase portrait of linear systems. a) Stable b) Unstable.

For a control system, a change in the set point is tantamount to shifting the stability state from 0 on the phase plane portrait to A as shown in Figure 3 (a). 0 now represents the minimum energy level of the system required for stability. It follows that the controller action will appear like it will have to dissipate energy equivalent to that between A and 0.

The locus of the system state due to the controller action can not be strictly along the x-axis. While an infinite number of possible paths can lead the system from state A to 0, those that remain exclusively in the upper left quadrant, Figure 3 (a), correspond to overdamped responses and those that traverse the x -axis, Figure 3 (b), correspond to underdamped responses.

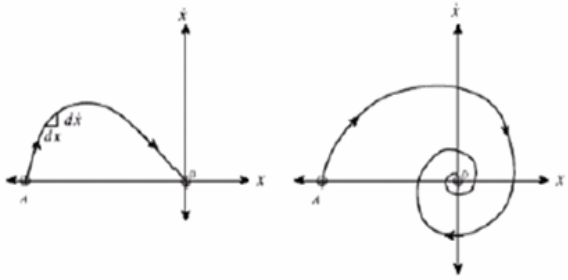

Figure 3: Control system with possible phase plane portrait a) Overdamped phase portrait b) Underdamped phase portrait.

A single structure conventional controller can be designed to allow energy to flow in one direction only resulting in an overdamped system. The system state in this case will remain in the second quadrant of the phase plane. Such a controller will not be optimal. Utkin [2] showed that a variable structure controller can be designed such that the phase plane portrait of the system will have a higher x yet remains entirely in the second quadrant. The energy based design methodology of such a controller is the subject of the next section.

3. Work and Energy Based VSC Design Methodology

With reference to Figure 4, the controller is required to move the system from (1) to (2) in the presence of a dissipative load. The work done by the controller less than that consumed by the dissipative load is related to the energy of the system as follows:

$$T_1 + V_1 + U_{1\to 2} = T_2 + V_2 + U_{R(1\to 2)} \quad (3)$$

where,

T_1, V_1 are the kinetic and potential energy at position (1).

T_2, V_2 are the kinetic and potential energy at position (2).

$U_{1\to 2}$ is the work done by the controller between the two positions.

$U_{R(1\to 2)}$ is the work lost due to the viscous damper between the two positions.

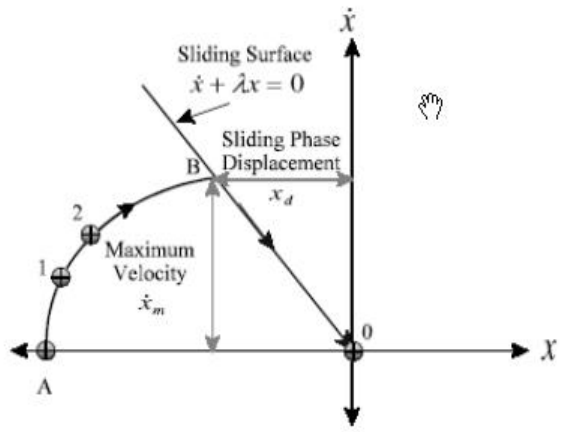

Figure 4: Phase plane portrait showing VSC action.

For a general system, Equation 3 becomes:

$$\tfrac{1}{2}\beta(\dot{x}_2^2 - \dot{x}_1^2) + \tfrac{1}{2}\alpha(x_2^2 - x_1^2) - \Gamma(\dot{x}_2 x_2 - \dot{x}_1 x_1) - k(x_2^2 - x_1^2) = 0 \quad (5)$$

β is the inertial energy storage element constant,

α is the potential energy storage element constant,

Γ is the linear dissipative element constant,

k is the controller gain.

As an example, consider a mechanical system given by the classical differential form:

$$m\ddot{x} + b\dot{x} + k_s x = u$$

Where *m*, *b*, and k_s are the mass, damping coefficient, and spring constant respectively. *u* is the controller force. The work done by the controller between (1) and (2) is given by:

$$\int_1^2 m\ddot{x}\,dx + \int_1^2 b\dot{x}\,dx + \int_1^2 k_s x\,dx = \int_1^2 u\,dx \quad (6)$$

Substituting $\ddot{x} = \dot{x}d\dot{x}/dx$, $u = kx$ and integrating gives:

$$\tfrac{1}{2}m(\dot{x}_2^2 - \dot{x}_1^2) + \tfrac{1}{2}k_s(x_2^2 - x_1^2) - b(\dot{x}_2 x_2 - \dot{x}_1 x_1) = \tfrac{1}{2}k(x_2^2 - x_1^2) \quad (7)$$

Comparing equation 4 and 7 shows that:

$\beta = m, \alpha = k_s$, and $\Gamma = b$

The energy balance at any point along the trajectory of the VSC phase portrait is given by:

$$\tfrac{1}{2}\beta\dot{x}^2 + \tfrac{1}{2}\alpha x^2 - \Gamma\dot{x}x - kx^2 = 0 \quad (8)$$

For the linear sliding surface shown in Figure 4, $x = -\dot{x}/\lambda$, substituting for *x* into equation 8 gives:

$$\tfrac{1}{2}\beta\dot{x}^2 + \tfrac{1}{2\lambda^2}\alpha\dot{x}^2 - \tfrac{1}{\lambda}\Gamma\dot{x}^2 = \tfrac{1}{\lambda}k\dot{x}^2 \quad (9)$$

Equation 9 relates the controller gain to the slope of the sliding surface as follows:

$$k = \tfrac{1}{2}(\beta\lambda^2 + \alpha) + \Gamma\alpha \quad (10)$$

Equation 10 can be used for SISO control systems. An extended design methodology can be achieved to include SIMO control systems. If a four-state-variables system with a single input is considered, two sliding surfaces can be designed as follows:

$$s_1 = \lambda_1 x_1 + x_2 \quad (11)$$

$$s_2 = \lambda_2 x_3 + x_4 \quad (12)$$

where x_1, x_2, x_3, and x_4 are the states of the system and $x_2 = \dot{x}_1$, and $x_4 = \dot{x}_3$.

The input control signal is a relay type signal and is given by:

$$u = k_1 x_1 + k_2 x_2 \quad (13)$$

where

$$k_1 = \begin{cases} +\eta_1, & sx_1 > 0 \\ -\eta_1, & sx_1 < 0 \end{cases} \quad (14)$$

and

$$k_2 = \begin{cases} +\eta_2, & sx_3 > 0 \\ -\eta_2, & sx_3 < 0 \end{cases} \quad (15)$$

λ_1, λ_2 are the slopes of the sliding surfaces

k_1, k_2 are the controller gains,

η_1, η_2 are the magnitudes of the controller gains.

Equation 10 can be used to find the magnitudes of the controller gains as well as the sliding surfaces slopes as follows:

$$k_1 = \tfrac{1}{2}(\beta_1\lambda_1^2 + \alpha_1) + \Gamma_1\alpha_1 \quad (16)$$

$$k_2 = \tfrac{1}{2}(\beta_2\lambda_2^2 + \alpha_2) + \Gamma_2\alpha_2 \quad (17)$$

The same methodology used before for finding the coefficient $\beta, \alpha,$ and Γ for both k_1 and k_2 is used as it will be shown later. Equations 16 and 17 show that the ranges of the VSC parameters $(\lambda_1, \lambda_2, k_1, k_2)$ are very wide such that additional constraints have to be imposed on the choice of the parameters. Sensitivity analysis [14] is introduced to find such constraints as it will be shown in the coming sections.

4. Inverted Pendulum System and VSCSCHEMES

Figure 5 shows an inverted pendulum system. Such systems are popular test cases and examples in many control literature because of the many practical applications they can model, particularly in the field of robotics and rockets [15]. The system is also found to be very informative for performance evaluation and comparison for various types of controllers. The goal for this system is to keep the pendulum always upright by controlling the input force applied to the cart.

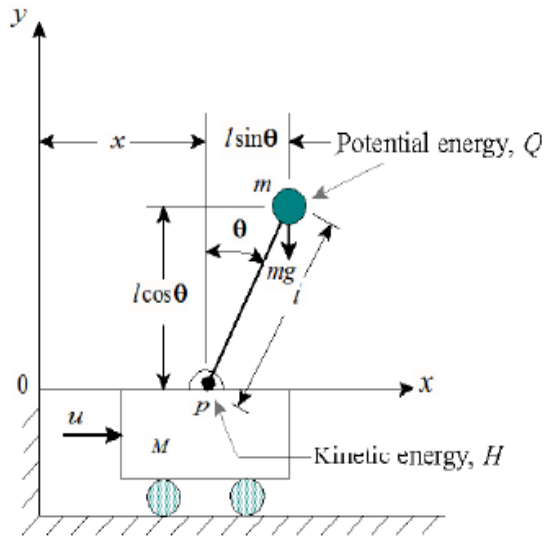

Figure 5: Inverted pendulum system.

With reference to Figure 5, the system has one input, the force u, and two outputs, the pendulum angle and the cart position x. The state space representation of the system dynamics, subject to the assumptions that the pendulum angular displacement is small and the angular velocity is negligible, is given as follows [16]:

$$\begin{bmatrix} \dot{x}_1 \\ \dot{x}_2 \\ \dot{x}_3 \\ \dot{x}_4 \end{bmatrix} = \begin{bmatrix} 0 & 1 & 0 & 0 \\ -\frac{m}{M}g & 0 & 0 & 0 \\ 0 & 0 & 0 & 1 \\ \frac{M+m}{MI}g & 0 & 0 & 0 \end{bmatrix} \begin{bmatrix} x_1 \\ x_2 \\ x_3 \\ x_4 \end{bmatrix} + \begin{bmatrix} 0 \\ \frac{1}{M} \\ 0 \\ -\frac{m}{MI} \end{bmatrix} u \qquad (18)$$

4.1. Controller Design Using Decoupled Sliding Surfaces:

The controller is designed such that motion along the sliding surfaces occurs independently as mention in Section 3. To bring the system back to stability at after a disturbance is difficult since only one control input is available. However, to guarantee this control task, two different sliding mode surfaces corresponding to the two desired system outputs and are used with one control signal u. Equations 11-17 can be used where and s are the sliding surfaces

In order to find the coefficients and for both and the methodology introduced in Section 3 is used, i.e., comparing Equations 16 and 17 to the system dynamics given by Equation 18 gives:

$$k_1 = \tfrac{1}{2} M \lambda_1^2 \qquad (19)$$

$$k_2 = \tfrac{1}{2} MI \lambda_2^2 + \tfrac{1}{2}(M+m)g \qquad (20)$$

Equations 19 and 20 show that choosing the values of the slopes and hence the corresponding control switching gains is difficult especially with the existence of cross coupling between the dynamics of the cart and that of the pendulum. The equations also show that for each of the two parts the value of one of the parameters λ_1 or k_1 has to be assumed. The ranges of the VSC variables are very wide as mentioned in Section 3. The system sensitivity to parameters variations is introduced to find parameter limitations. The condition $\dot{s} = 0$ is necessary to keep the system state on the sliding surface. Combining the system sensitivity with $\dot{s}_1 = 0$ and $\dot{s}_2 = 0$ for both sliding surfaces result in the following cases:

Case I: Sliding surface of the cart:

Since $s_1 = \lambda_1 x + \dot{x}$, the rate of change of sliding surface equation $\dot{s}_1$ is given by:

$$\lambda_1 \dot{x} + \ddot{x} = 0 \qquad (21)$$

Substituting for *u* and *x* from Equations 13 and 18 into Equation 21 respectively results in the following:

$$\lambda_1 \dot{x} + \tfrac{1}{M} k_1 x + (\tfrac{1}{M} k_2 - \tfrac{mg}{M})\theta = 0 \qquad (22)$$

The change in the angular position θ of the inverted pendulum system, and hence its stability, to changes in the cart velocity $\dot{x}$ is obtained from the partial derivative of θ with respect to x as follows:

$$\frac{\partial \theta}{\partial \dot{x}} = -\frac{M \lambda_1}{k_2 - mg} \qquad (23)$$

For the pendulum position θ to be rendered insensitive to the cart velocity $\dot{x}$, the magnitude of the denominator of Equation 23 must be much larger than that of the numerator. This implies $\lambda_1 << (k_2 - mg)/M$.

Substituting for λ_1 and then for k_2 from Equations 19 and 20 respectively into Equation 23 gives the following two

$$k_1 << \frac{(k_2 - mg)^2}{2M} \qquad (24)$$

$$\lambda_1 << \tfrac{1}{2} l \lambda_2^2 + \frac{1}{2M}(M-m)g \qquad (25)$$

Case II: Sliding surface of the cart:

Since $s_2 = \lambda_2 \theta + \dot{\theta}$ and the rate of change of sliding surface equation $\dot{s}_2$ is given by:

$$\lambda_2 \dot{\theta} + \ddot{\theta} = 0 \qquad (26)$$

Substituting Equations 13 and 18 into Equation 26 for u and $\ddot{\theta}$ gives:

$$\lambda_2 \dot{\theta} + \left[\frac{(M+m)g}{MI} - \frac{k_2}{MI}\right]\theta - \frac{k_1}{MI} x = 0 \qquad (27)$$

It can be seen that Equation 27 provides no significant information. Also, it is not possible to carry out the sensitivity analysis since the equation does not include the cart velocity.

4.1.1. Simulation Results and Comparisons:

In this section, a proportional controller and a VSC based on the new design methodology are applied to the inverted pendulum system for comparison. Table 1 shows the values of the system parameters used.

Table 1: Inverted pendulum numerical values.

m	*0.1 kg*
M	*2 kg*
I	*0,5 m*
g	*9.81 m/sec²*

Substituting the parameters of Table 1 into Equations 19 and 20 gives:

$$k_1 = \lambda_1^2 \tag{28}$$

$$k_2 = \tfrac{1}{2}\lambda_2^2 + 10.3 \tag{29}$$

With reference to Figure 5, in order to find the optimal limits of Equations 28 and 29, the pendulum is disturbed by applying an initial input angle. The pendulum at this inclination has a maximum potential energy *Q* that must be compensated for by the kinetic energy *H* in order to keep the system at that inclination stable, hence;

$$Q = H \tag{30}$$

$$mgl = \tfrac{1}{2}(M+m)\dot{x}^2$$

For a maximum initial disturbance angle $\theta = -0.1 rad\ (5.73^\circ)$ and the parameters of Table 1, Equation 30 results in $\dot{x} = 0.683 m/\sec$; consequently, $\dot{\theta} = 1.366 rad/\sec$ and the slope of the sliding surface becomes:

$$\lambda_2 = \frac{\dot{\theta}}{\theta} = \frac{1.336}{0.1} = 13.66 \sec^{-1} \tag{31}$$

Equations 28 and 29 are used with the constraints found from the sensitivity analysis to design the VSC. The slope of the cart sliding surface λ_1 must satisfy the condition of Equation 25. For $\lambda_2 = 13.66 \sec^{-1}, \lambda_1 << 51.3 \sec^{-1}$, λ_1 is selected to be 0.7 and result in the corresponding controller gains $k_1 = \pm 0.49$ and $k_2 = \pm 103.6$. These values do satisfy the constraint set forth by Equation 24. The responses of the pendulum and cart with respect to time for this design case are shown in Figures 6 and 8 respectively. The corresponding phase portraits are shown in Figures 7 and 9 respectively.

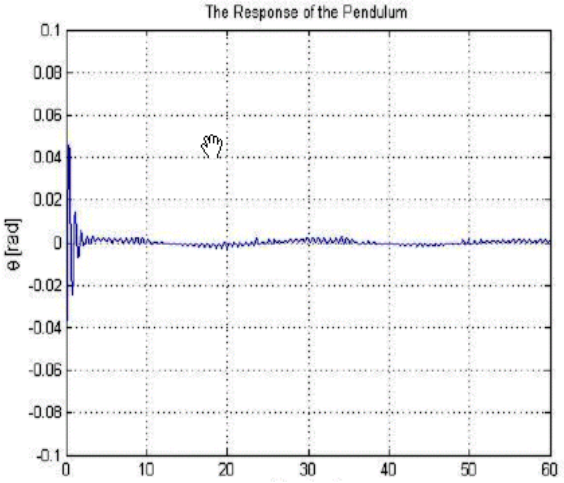

Figure 6: Pendulum response for VSC.

The system state crosses the sliding surface at relatively high speed such that it leaves the sliding surface as shown in Figure 7. Since the structure of the controller is unable to brake the system, the system circles around the origin and intercepts the sliding surface in the lower right quadrant. In Figure 6, this is manifested by the oscillations of the pendulum around the set point. With reference to the cart, when the pendulum is disturbed by the initial input angle, the cart tries to compensate by moving in the same direction of the input angle as shown in Figure 9.

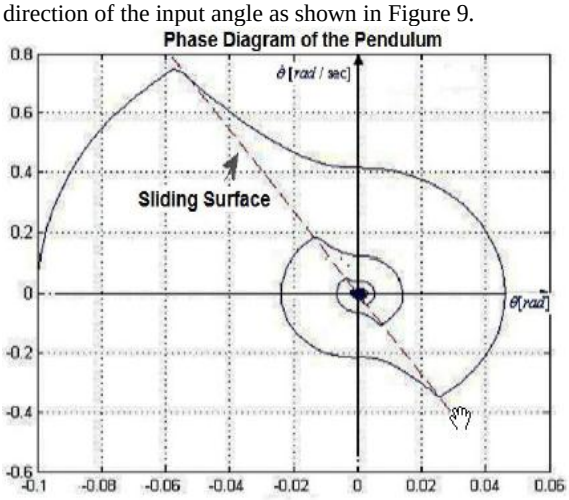

Figure 7: Pendulum phase portrait for the VSC.

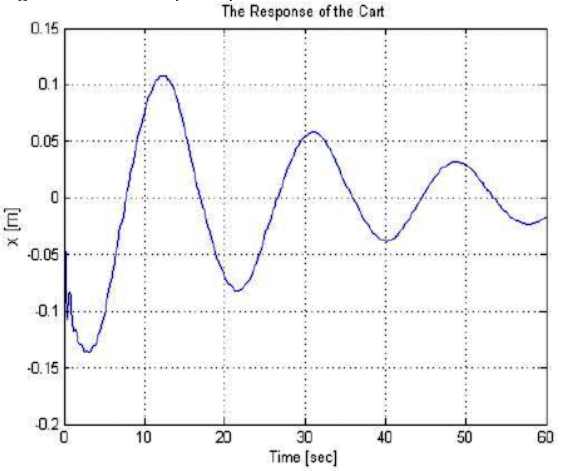

Figure 8: Cart response for the VSC.

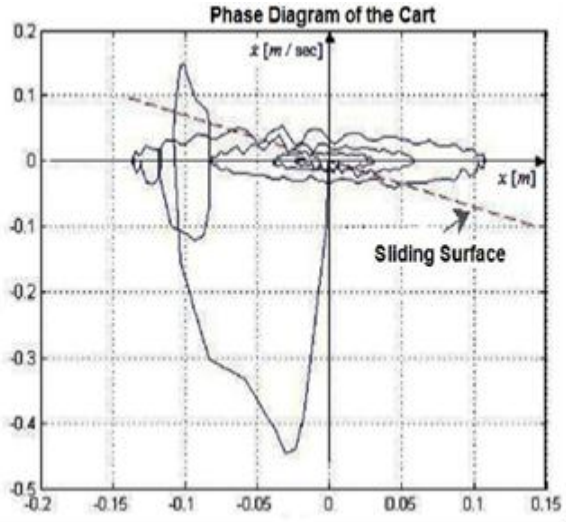

Figure 9: Cart phase portrait for the VSC.

While returning back to its original position, the cart oscillates around the origin in response to the oscillatory behavior of the pendulum in order to keep it stable upright as shown in Figure 8. This is manifested on the phase diagram whereby its response leaves the sliding surface of the cart while stabilizing the pendulum and returning back to the original position represented by the origin of the plot.

Reducing the slopes of the cart and the pendulum sliding surfaces to respectively results in the responses and the phase portraits shown in the Figures 10-13. In this case, the response of the pendulum is marginally underdamped, and the pendulum will keep oscillating with a small magnitude around the equilibrium point. The response of the cart in this case is overdamped. Reducing the slopes implies reducing the kinetic energy when the system state intercept the sliding surfaces for the pendulum and the cart. The system state do not leave the sliding surface as shown in Figures 11 and 13.

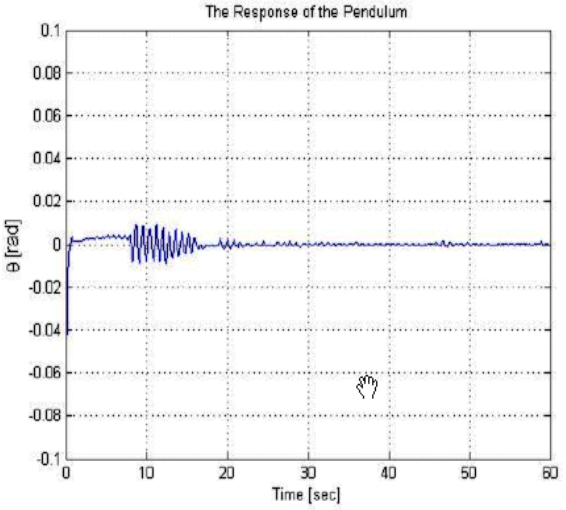

Figure 10: Pendulum response for the VSC.

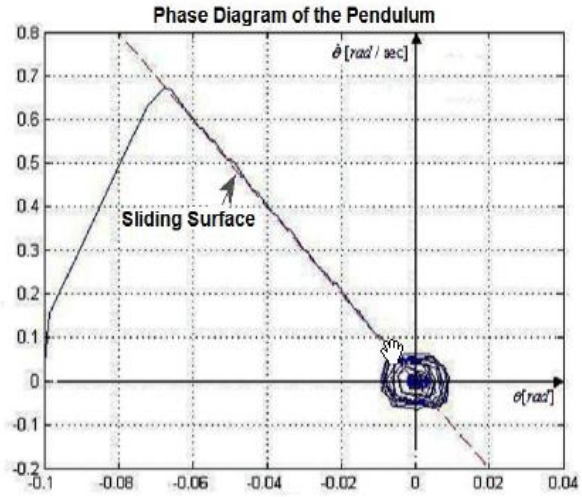

Figure 11: Pendulum phase portrait.

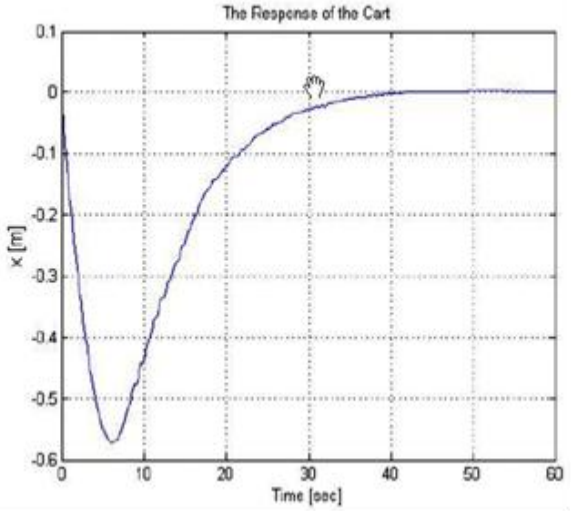

Figure 12: Cart response for the VSC.

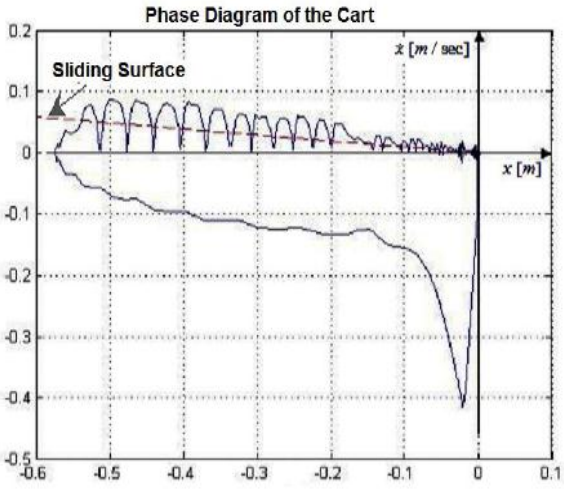

Figure 13: Cart portrait for the VSC.

Since the system is a single-input-two-output, a possible proportional control law can be constructed as follows:

$$u = k_1 x + k_2 \theta \tag{32}$$

where k_1 and k_2 are the controller gains.

If the proportional controller gains are selected to be where $k_1 = 0.49$ and $k_2 = 103.6$ are the responses of the pendulum and the cart for the same step input used earlier are shown in Figures 14 and 16 respectively. The corresponding phase portraits are shown in Figures 15 and 17 respectively. The figures show critically stable undamped responses. The performance of the VSC and the proportional controller based on the simulation results clearly show how the energy is absorbed by VSC as it asymptotically brings the system to stability, while it is not the case when the proportional controller is used.

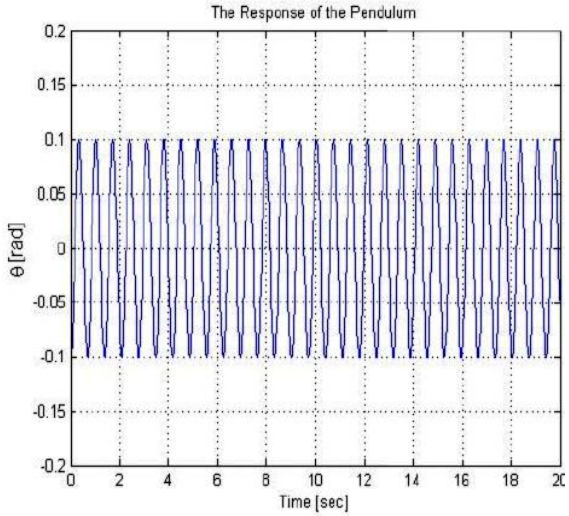

Figure 14: Pendulum response for the P-controller.

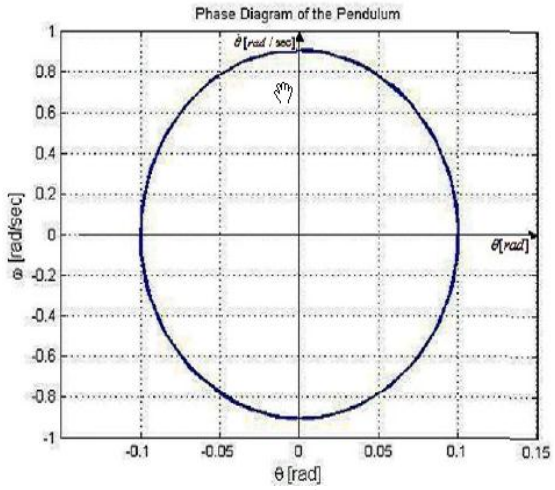

Figure 15: Pendulum phase portrait for the P-controller.

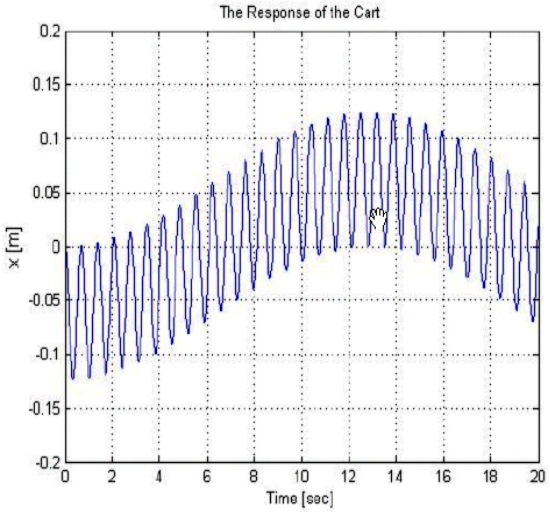

Figure 16: Cart response for the P-controller.

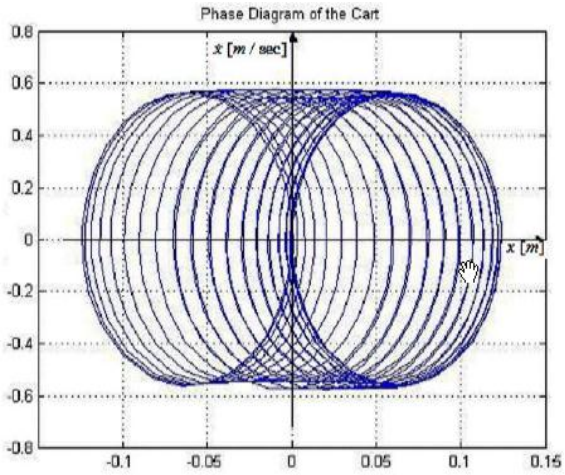

Figure 17: Cart phase portrait for the P-controller.

4.2. Controller Design Using Hyper Sliding Surface:

The sliding mode controller in this section is designed such that the sliding surfaces of the pendulum and the cart are coupled together to form a hyper sliding surface. The hyper sliding surface has the following form:

$$s = s_1 + s_2 \tag{33}$$

where s_1 and s_2 are the sliding surfaces of the pendulum and the cart respectively. Substituting Equations 11 and 12 for s_1 and s_2 in to Equation 33 gives:

$$s = \lambda_1 x + \dot{x} + \lambda_2 \theta + \dot{\theta} \tag{34}$$

The input force applied to the cart *u* is a relay type signal and is given by:

$$u = \begin{cases} +v, & s > 0 \\ -v, & s < 0 \end{cases} \tag{35}$$

where the values of $+v$ and $-v$ are chosen based on the system capability.

4.2.1. Simulation Results and Comparisons:

If a DC motor is used to provide the desired input force u to the cart, the selection of the values and is based on the motor torque limits. The rated torque of the motor can be chosen to be 0.28 N.m. [16] and a gear ration of 1:16. If the cart wheel connected to the motor has a radius of 5cm, the controller force will have switching gains ±90. For the same sliding surfaces used in Section 3.1, , Figures 18 and 19 show the responses of the pendulum and cart respectively. The performance of this controller is much better than those of the previous controller. The pendulum response is faster than the one shown in Section 4.1 and is marginally underdamped (around the critical damping state). The cart response shows an underdamped response with a small overshoot; however, it is faster than the one of Section 4.1.

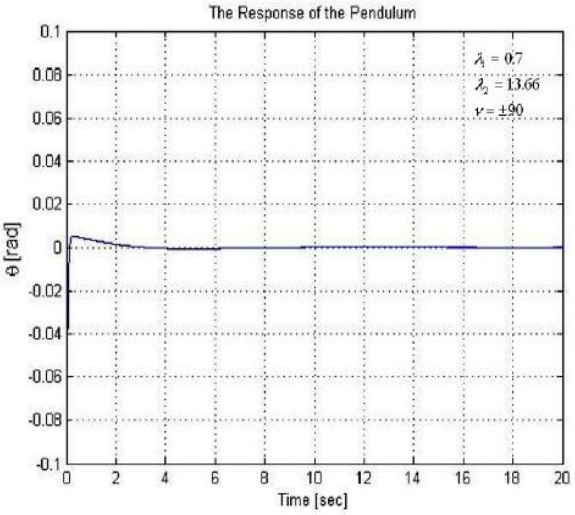

Figure 18: Pendulum response for the Hyper VSC.

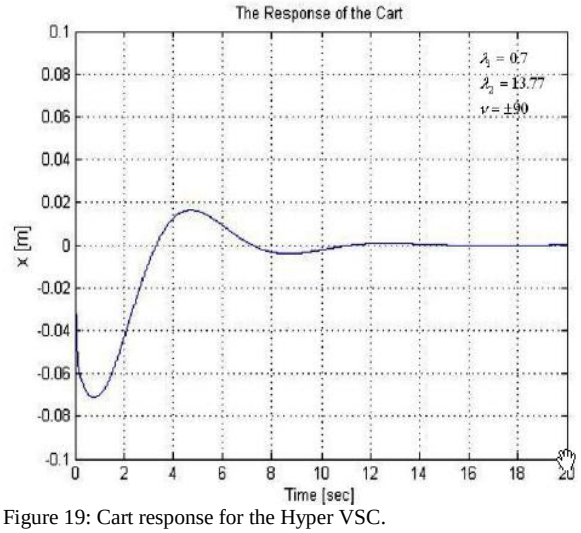

Figure 19: Cart response for the Hyper VSC.

4.3. Controller Design of Pure Inertial System:

The inverted pendulum system has no dissipative viscous load to absorb energy. This can be seen in the dynamic equations of the system. The controller design used in Section 3 also does not include any damping terms in the control law to compensate for the lack of damping. Hence, adding a damping terms in the control law is advisable. This can be accomplished by modifying the control law of Equation 13 as follows:

$$u = k_1 x + k_2 \theta + k_3 \dot{x} + k_4 \dot{\theta} \tag{36}$$

where k_1 and k_2 are the same controller gains given by Equations 14 and 15. k_3 and k_4 are the damping controller gains, and chosen to be always positive. In order to select suitable values for k_3 and k_4 the system sensitivity analysis is carried out as follows:

$$\left(\lambda_1 + \frac{k_3}{M}\right)\dot{x} + \frac{k_1}{M} x + \frac{k_3 - mg}{m}\theta + \frac{k_4}{M}\dot{\theta} = 0 \tag{37}$$

Taking the partial derivative of the pendulum angle with respect to the cart velocity in Equation 37 gives:

$$\frac{\partial \theta}{\partial \dot{x}} = \frac{M\lambda_1 + k_3}{k_2 - mg} \tag{38}$$

Case I: Sliding surface of the pendulum:

Substituting Equations 18 and 36 into Equation 26 for $\ddot{\theta}$ and *u* respectively gives:

$$-\frac{k_1}{Ml} x - \frac{k_3}{Ml}\dot{x} + \frac{(M+m)g - k_2}{Ml}\theta + \left(\lambda_2 - \frac{k_4}{M}\right)\dot{\theta} = 0 \tag{39}$$

Taking the partial derivative of the pendulum angle with respect to the cart velocity in Equation 39 gives:

$$\frac{\partial \theta}{\partial \dot{x}} = \frac{k_3}{k_2 - (M+m)g} \tag{40}$$

In order for the system to be rendered insensitive to the cart velocity, the magnitude of the denominators of Equations 38 and 40 must be much larger than that of the numerators, hence:

$$k_3 << k_2 - mg - M\lambda_1 \tag{41}$$

$$k_3 << k_2 - (M+m)g \tag{42}$$

If the partial derivative of the pendulum angular velocity is taken with respect to the cart velocity in Equations 37 and 39, the following can be achieved:

$$\frac{\partial \dot{\theta}}{\partial \dot{x}} = \frac{M\lambda_1 + k_3}{k_4} \tag{43}$$

$$\frac{\partial \dot{\theta}}{\partial \dot{x}} = \frac{k_3}{k_3 - \lambda_1 Ml} \tag{44}$$

With reference to Figure 5, the following equation is also valid:

$$\frac{\partial \dot{\theta}}{\partial \dot{x}} = \frac{1}{l} \tag{45}$$

Equating Equation 43 and 44 to Equation 45 respectively gives

$$k_4 = -(lk_3 + Ml\lambda_1) \tag{46}$$

$$k_4 = lk_3 + Ml\lambda_2 \quad (47)$$

Equation 46 can be ignored since k_4 is chosen to be always positive.

4.3.1. Simulation Results and Comparisons:

In order to use the control law of Equation 36, the controller gains k1, k2, k3, and k4 must be selected based on the sensitivity analysis of the system. With reference to Section 4.1, the slope of the cart sliding surface must satisfy the condition of Equation 25.. Substituting and into Equations 28 and 29 result in the corresponding controller gains k1 = ±4 and k2 = ±103.6 respectively. The damping controller gains k3 and k4 must satisfy the conditions of Equations 41, 42, and 47. Since k3 << 82.7, k3 is selected to be 9. Substituting the parameters in Table 1 into Equation 47 with k3 = 9 results in k4 = 18.16. Figures 20 and 21 show the responses of the pendulum and the cart respectively. The response of the cart is overdamped and the response of the pendulum is marginally underdamped.

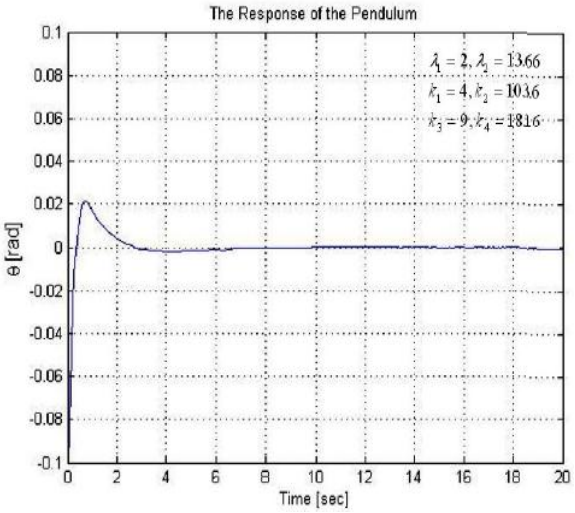

Figure 20: Pendulum response for the modified VSC of pure inertial systems.

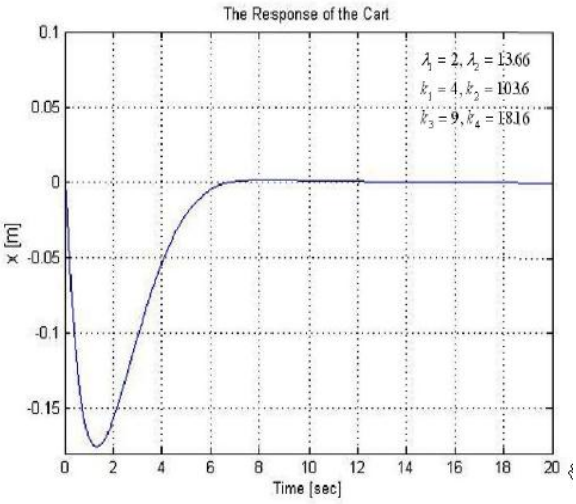

Figure 21: Cart response for modified VSC of pure inertial systems.

For comparison purposes, a Proportional-Derivative (PD) controller design that has the following form is used [16]:

$$u = 163.1x + 73.4\dot{x} + 298.15\theta + 60.7\dot{\theta} = 0 \quad (48)$$

The PD-controller gains of Equation 48 are chosen based on the pole placement tuning method where the closed loop pole locations are selected to meet a given desired performance specifications. The closed-loop pole locations are chosen to give a 2 sec settling time [16]. The responses of the pendulum and the cart when using this controllers are shown in Figures 22 and 23. The figures show that both responses are underdamped. The 2 sec settling time results in 0.5 damping ratio and 70% overshoot as shown in Figure 22.

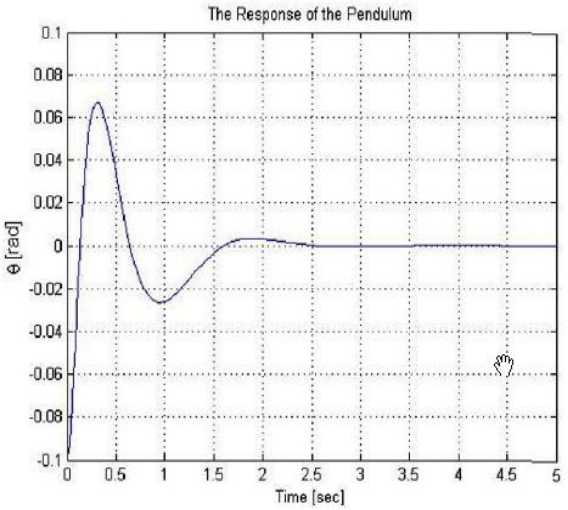

Figure 22: Pendulum response of PD-controller [16].

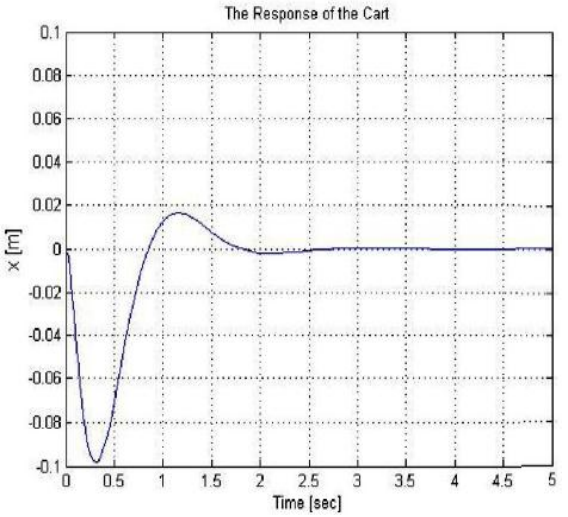

Figure 1: Cart response for the PD-controller [16].

A faster response of the pendulum alone ignoring completely the cart can be obtained if the choice of the PD-controller gains of the pendulum are selected based on Ziegler-Nichols method of tuning [16]. The control law in this case is given by:

$$u = 210\theta + 10.5\dot{\theta} \quad (49)$$

Figure 24 shows the response of the pendulum in this case. Figure 25 shows the cart response to continually

move away from the desired equilibrium state since there is no contribution of the cart state in the control law. If the control law (Equation 49) is modified to include the cart state, and the gains of these state are tuned using the MATLAB Control System Toolbox, the following control law is obtained:

$$u = 15x + 5\dot{x} + 210\theta + 10.5\dot{\theta} \quad (50)$$

Figure 24 also shows the pendulum response when using this modified PD-controller. The figure shows the response to be more oscillatory, however, with reference to Figure 25 the cart response is shown to be stable but slightly underdamped. When MATLAB Control System Toolbox is used to tune the PD-controller gains of both cart and pendulum together, the following control low results:

$$u = 80x + 100\dot{x} + 550\theta + 82\dot{\theta} \quad (51)$$

The response of the pendulum using the control law of Equation 51 is underdamped as shown in Figure 24. The cart response in this case however, is overdamped as shown in Figure 25.

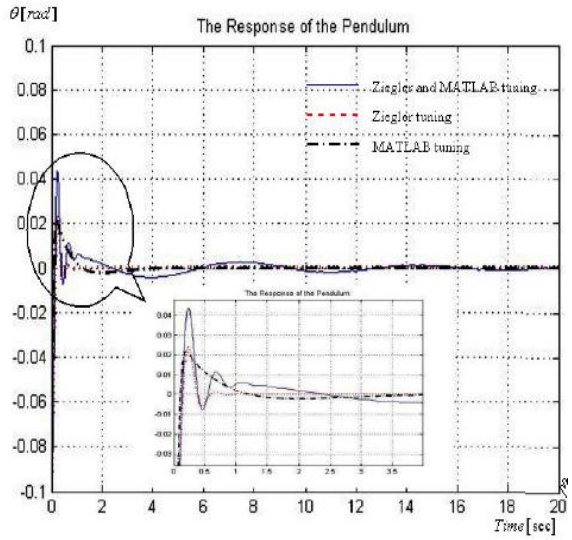

Figure 24: Pendulum response using different PD tuning.

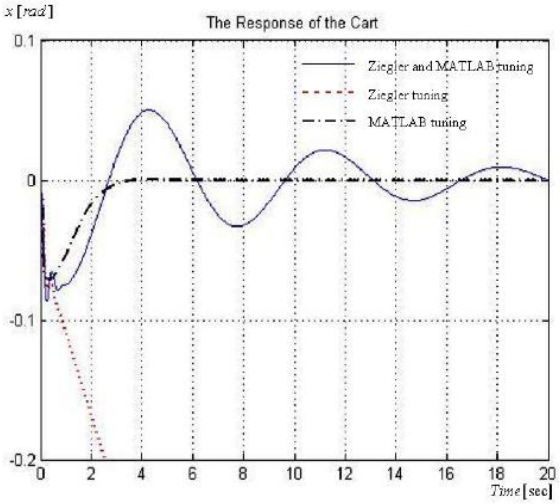

Figure 25: Cart responses using different tuning methods for PD-controllers.

Comparing the responses of the different controllers used so far shows that the PD-controller of Equation 48 has the fastest response for the cart; however, the response has an overshoot. The response of the system when using the VSC with the hyper sliding surface shows ideal performance for the pendulum where the response is almost at the critical damping state, and is faster than for all the other types of controllers. Comparing the responses of the cart and the pendulum for the original VSC of Equation 13 with that of the modified VSC of Equation 36 shows that the modified VSC has a better performance and a faster response. The response of the cart for the modified VSC also shows a faster response and a better performance than that of the VSC with a hyper sliding surface.

Among the four PD-controllers, that of Equation 49 results in the best performance of the pendulum, least overshoot and the fastest response. Comparing this performance to that of the VSC with the hyper sliding surface shows that the latter is still the best among all controllers. The cart response when using the controller of Equation 51 is faster than those resulting from using other controllers, and has no overshoot.

5. Conclusion

This paper presents the derivation and the proof of the relationship between a system's work and energy and a VSC to control it. The relationship between the slope of the linear sliding surface and the controller gains is then used to develop a simple systematic design methodology suitable for SISO systems. This new design methodology is then extended to SIMO systems. An inverted pendulum system is used to test this new design methodology. The results show that the proposed approach produces a controller with very good performance. In order to enhance further the performance, a hyper VSC was applied; where the sliding surfaces of the pendulum and cart are coupled together. Since the pendulum systems is a pure inertial system, the control law was improved upon by introducing artificial damping terms. The VSC schemes simulation results were compared to those of a proportional and a PD-controller. The comparison shows that the performance of the VSC with the hyper sliding surface is the best among all controllers.

References

[1] Yu-Fing Li, "High Precision Motion Control Based on Discrete Time Sliding Mode Approach", Doctoral Thesis, Royal Institute of Technology, Stockholm, Sweden, 2001.

[2] Jeen Lin, Ruey-Jing Lian, "Enhanced fuzzy sliding mode controller for active suspension systems", IEEE Transactions on Automatic Control, Volume 19, Issue 7, Pages 1178-1190, 2009.

[3] J. Slotine, W. Li, "Applied Nonlinear Control", Prentice Hall Englewood Cliffs, New Jersey, 1992.

[4] Qinglei Hu, "Variable structure maneuvering control with time-varying sliding surface and active vibration damping of flexible spacecraft with input saturation", Acta Astronautica, , Volume 64, Issues 11-12, June-July 2009.

[5] M.Ö. Efe, "MIMO variable structure controller design for a bioreactor benchmark process", ISA Transactions, Volume 46, Issue 4, Pages 459-469, 2007.

[6] J. Ackermann, V. Utkin, "Sliding Mode Control Design Based on Ackermann's Formula", IEEE Transactions on Automatic Control, Vol. 43, Issue 2, pp. 234-237, Feb. 1998.

[7] K. Young, V. Utkin, U. Ozguner, "Sliding mode control for a class of non-affine nonlinear systems", Nonlinear Analysis: Theory, Methods & Applications, Volume 71, Issue 12, Pages e1589-e1597, 15 December 2009.

[8] Tai-Zu Wu, Jinn-Der Wang, Yau-Tarng Juang, "Decoupled integral variable structure control for MIMO systems", Journal of the Franklin Institute, Volume 344, Issue 7, Pages 1006-1020, October 2007.

[9] İlyas Eker, "Sliding mode control with PID sliding surface and experimental application to an electromechanical plant", ISA Transactions, Volume 45, Issue 1, Pages 109-118, January 2006.

[10] J. Wang, A. B. Rad, P. T. Chan, "Indirect Adaptive Fuzzy Sliding Mode Control: Part I: Fuzzy Switching", Journal of Fuzzy Sets and Systems, Vol. 122, Issue 1, pp.21-30, 2001.

[11] H.F. Ho, Y.K. Wong, A.B. Rad "Adaptive fuzzy sliding mode control with chattering elimination for nonlinear SISO systems", Simulation Modelling Practice and Theory, Volume 17, Issue 7, Pages 1199-1210, August 2009.

[12] S.M. Gadoue, D. Giaouris, J.W. Finch, "Artificial intelligence-based speed control of DTC induction motor drives—A comparative study", Electric Power Systems Research, Volume 79, Issue 1, Pages 210-219, January 2009.

[13] J. Javadi Moghaddam, M.H. Farahani, N. Amanifard, "A neural network-based sliding-mode control for rotating stall and surge in axial compressors", Applied Soft Computing, In Press, Corrected Proof, Available online 11 February 2010.

[14] R. C. Dorf, Robert H. Bishop, "Modern Control Systems", 11th Edition, Prentice Hall, New Jersey 2008.

[15] E. Doskoscz, Y. Shtessel, "MIMO Sliding Mode Control of a Robotic 'Pick and Place' System Modeled as an Inverted Pendulum on a moving Car", IEEE Proceedings of the Southeastern Symposium of System theory, 1998.

[16] K. Ogata, "Modern Control Engineering", 5th Edition, Prince Hall, New Jersey, 2010.